Journal of Catalysis 269 (2010) 376–387

Contents lists available at ScienceDirect

Journal of Catalysis

journal homepage: www.elsevier.com/locate/jcat

Preparation, characterization, and kinetic evaluation of dendrimer-derived bimetallic Pt–Ru/SiO_2 catalysts

Dongxia Liu, Yaritza M. López-De Jesús, John R. Monnier, Christopher T. Williams *

Department of Chemical Engineering, Swearingen Engineering Center, University of South Carolina, Columbia, SC 29208, United States

ARTICLE INFO

Article history:
Received 22 July 2009
Revised 19 November 2009
Accepted 23 November 2009
Available online 31 December 2009

Keywords:
Platinum
Ruthenium
Bimetallic
Dendrimer
Nanoparticle
3,4-Epoxy-1-butene
Hydrogenation

ABSTRACT

A series of silica-supported Pt, Ru, and Pt–Ru catalysts has been synthesized using dendrimer–metal nanocomposite (DMN) precursors prepared by both co- and sequential complexation with metal salts. The catalysts have been characterized by several techniques, including electron microscopy, temperature-programmed titration of adsorbed oxygen, and X-ray diffraction. Liquid-phase selective hydrogenation of 3,4-epoxy-1-butene (EpB) was used as a probe reaction to evaluate their catalytic performance. The bimetallic catalyst prepared by the co-complexation method exhibits a superior catalytic activity compared to the sequential one, and is much more active than a conventional catalyst prepared by incipient wetness. The activity enhancement is attributed to a bifunctional performance of the PtRu alloy sites created, based on a strong correlation between turnover frequencies, and both the alloy compositions and metal surface site distributions. In addition, the co-complexation catalyst is selective toward crotonaldehyde, suggesting that this reaction pathway is favored on the PtRu sites.

1. Introduction

Over the years, bimetallic or multi-metallic catalysts have replaced many monometallic catalysts in industrial applications due to the superior activities and/or selectivities that can be achieved. Such enhanced performance can be contributed to a combination of geometric, electronic, and/or bifunctional effects [1–3]. Preparation of bimetallic or multi-metallic catalysts usually involves co-impregnation or successive impregnation methods. However, these traditional preparation methods often provide unsatisfactory control over the dispersion of the metal atoms, resulting in homogeneity problems such as metal segregation, sintering, and surface enrichment of the "inactive" metal.

One promising method of preparing bi- or multi-metallic catalysts with uniform composition is using dendrimers as templates and stabilizers. Dendrimers [4,5] are mono-disperse, hyperbranched polymers that emanate from a central core with repetitive branching units. While possessing a very dense exterior, they contain hollow pockets that can be ideal for use as nano-scale containers. The use of dendrimers as templates/stabilizers for the synthesis of nanoparticles is a relatively new but active field. One of the more successful applications along these lines has been the synthesis of metal nanoparticles using poly-(amidoamine) (PAMAM) dendrimers. Originally pioneered by Crooks et al. [6], the approach takes advantage of the fact that transition metal ions (e.g., Pt^{2+}, Cu^{2+}, and Pd^{2+}) can coordinate with the interior amine groups of the dendrimer. Such ions may then be reduced to form dendrimer–metal nanocomposites (DMNs) that are stable for extended periods of time and can exhibit interesting catalytic properties [7]. The dendrimer can exert control over size and (in the case of multiple metal ions) composition of the resulting nanoparticles or clusters, which can allow for tuning of catalytic properties.

There are now many investigations exploring the use of DMNs as precursors to synthesize supported catalysts [8–16], although still relatively few examples for bimetallic Pt-based systems. For example, Lang et al. [17] have examined the possibility of preparing dendrimer-templated, supported Pt–Au bimetallic nanoparticles using the displacement reaction method. In this approach, Cu^0 nanoparticles complexed with dendrimer amine groups are exchanged with a mixture of Pt(II) and Au(III) in solution, thus forming zero valent Pt–Au nanoparticles. Hoover et al. [18] synthesized PAMAM dendrimer-templated Pt–Cu bimetallic nanoparticles supported on alumina that were tested as heterogeneous catalysts for CO oxidation and toluene hydrogenation reactions. Xie and coworkers [13] reported the synthesis of bimetallic Pt–Cu catalysts supported on silica using dendrimer-templating methods. They observed a synergistic catalytic effect on activity for hydrodechlorination of 1,2-dichlorethane, which was attributed to bifunctional bimetallic Pt–Cu sites.

Liquid-phase selective hydrogenation of the multi-functional olefin 3,4-epoxy-1-butene (EpB) is an interesting probe reaction

* Corresponding author. Fax: +1 (803) 777 8265.
E-mail address: willia84@cec.sc.edu (C.T. Williams).

0021-9517/$ - see front matter © 2009 Elsevier Inc. All rights reserved.
doi:10.1016/j.jcat.2009.11.021

to examine the kinetic performance of bimetallic catalysts. EpB has both a C=C bond and an epoxy group, and in the presence of metal catalysts and hydrogen can proceed via isomerization, hydrogenation, and/or hydrogenolysis reactions to form a range of reaction products. The reaction scheme for selective hydrogenation/hydrogenolysis of EpB is shown in Fig. 1. Several transition metals have been tested as catalysts for EpB hydrogenation and/or hydrogenolysis reactions [19–26]. Pt [19,23] and Rh [22,25] favor C=C bond hydrogenation, with the former being less selective. Pd [19,21] is especially active toward the rupture of the epoxy group to form stable π-allylic intermediates. The deoxygenation reaction to form 1,3-butadiene is favored over Cu catalysts [20]. So far, the catalytic performance of Ru has not been studied for EpB hydrogenation; likewise, no bimetallic systems other than Pt–Ag [24] and Cu–Pd [26] have been explored.

In this study, a family of dendrimer-derived Pt–Ru catalysts has been prepared to illustrate dendrimer-templating effects on bimetallic structure and correlate physical and/or chemical properties of the bimetallic catalysts with their kinetic behavior for EpB hydrogenation. It was found that dendrimer-derived bimetallic catalysts exhibited different metal nanoparticle sizes and distributions when compared with conventionally prepared samples. In addition, Pt–Ru alloy sites are maximized using the dendrimer templating co-complexation method, resulting in an enhanced activity and unusual selectivity to crotonaldehyde.

2. Materials and methods

2.1. Materials

Fourth generation hydroxyl-terminated poly(amido)amine (PAMAM) dendrimer (G4OH) (10 wt% in methanol solution) was obtained from Aldrich. Prior to use, an aqueous solution was made by evaporating methanol with flowing N_2 and diluting the residue to 4.2×10^{-4} M with deionized water. $RuCl_3{\cdot}xH_2O$ (99.98 % Ru, Aldrich), $H_2PtCl_6{\cdot}6H_2O$ (99.9%-Pt, Strem Chemicals), and $NaBH_4$ (granules, 99.995%, Aldrich) were used as received. Deionized water (18 MΩ cm Milli-Q) was used to prepare all the aqueous solutions. Silica support (specific surface area = 67 m^2/g, pore volume = 1.3 mL/g) was supplied by BASF Catalysts LLC. Crotonaldehyde (99.5%, Aldrich) and 3,4-epoxy-1-butene (EpB) (Eastman Chemical Company) were used as received. Hexane (99.5% purity minimum, HPLC grade) was purchased from VWR. Oxygen (UHP), helium (UHP), and hydrogen (UHP) were supplied by Airstar.

2.2. Catalyst preparation

The synthesis of dendrimer–metal nanocomposites was adapted from the literature [6] and has been published before. [12] A proper amount of 3.96×10^{-3} M $RuCl_3{\cdot}xH_2O$ precursor solution was added under the N_2 purging to G4OH dendrimer solution with the concentration of 4.2×10^{-4} M to reach a molar ratio of Ru^{3+} to G4OH of 40:1. The mixed solution was stirred for 3 days at room temperature with N_2 flowing to protect the Ru^{3+} ions from oxidation by dissolved O_2 and allow the complexation of Ru^{3+} ions with the functional groups in G4OH dendrimer. Freshly made 0.1 M $NaBH_4$ aqueous solution was then added to the dendrimer–Ru nanocomposites, yielding a mass ratio of $NaBH_4$ to metal of 1:1, to attempt to reduce the incorporated Ru^{3+} ions to Ru nanoparticles. The reduction procedure lasted for at least 30 min with mild stirring until there were no more H_2 bubbles generated. The supported catalyst was made by standard wet impregnation of the reduced dendrimer–Ru nanocomposite onto SiO_2 to a nominal Ru loading of 0.52 wt%. The extra water was removed under ambient conditions by evaporation of the stirring slurry for 3 days. The same procedure was used to make dendrimer–Pt monometallic nanocomposites, with the corresponding supported catalyst having a nominal Pt loading of 1 wt%. The only difference was that the concentration of $H_2PtCl_6{\cdot}6H_2O$ aqueous precursor solution was 2.05×10^{-3} M.

Two synthesis routes were used to produce bimetallic Pt–Ru DMNs, as shown in Fig. 2. The co-complexation method involved adding an equal molar amount of the two metal precursor solutions simultaneously to dendrimer solution. The resulting solution was allowed to complex for 3 days under N_2 purging and subsequently reduced with $NaBH_4$. The sequential method involved first mixing one metal precursor solution with the dendrimer solution, followed by reduction after complexation was completed. Then, the second metal precursor solution was added, whereupon complexation with the second metal occurred, followed once again by reduction with $NaBH_4$. The first metal was Pt, while the second was Ru. For both methods, the target ratio of each type of metal atom to dendrimer was 20:1, thus making a total metal atom loading of 40 atoms per dendrimer, as for the monometallics. The dendrimer–Pt–Ru bimetallic nanocomposites made by both

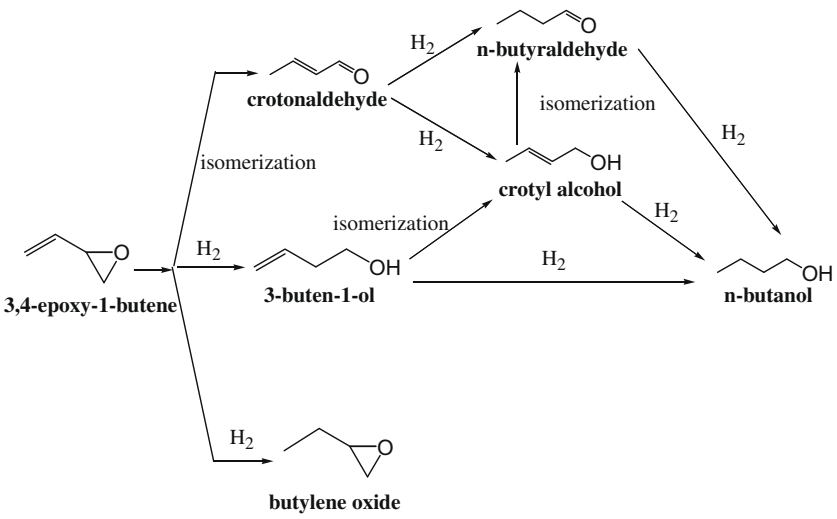

Fig. 1. Reaction scheme of selective hydrogenation/hydrogenolysis of 3,4-epoxy-1-butene.

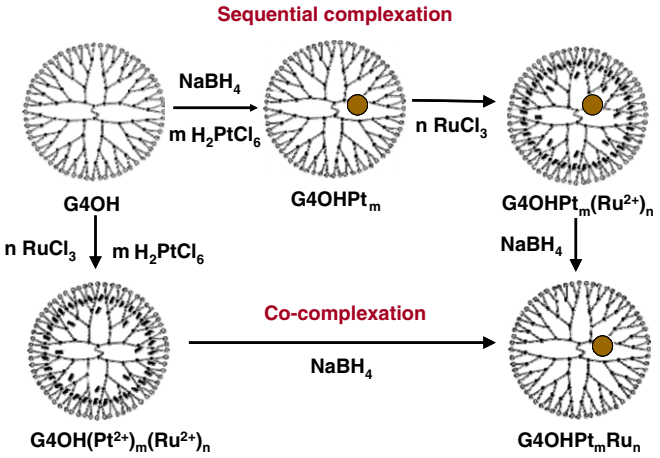

Fig. 2. Schematic of Pt–Ru DMN precursor synthetic routes.

co-complexation and sequential methods were impregnated onto silica as described above, with the nominal loading of 0.5 wt% Pt and 0.26 wt% Ru.

Conventional Pt and Ru catalysts were made by incipient wetness method. A proper amount of 3.94×10^{-2} M of $RuCl_3{\cdot}xH_2O$ precursor solution was added dropwise to SiO_2 and the resulting slurry was dried in an oven at 100 °C for 2 h before use. A conventional Pt catalyst was made with exactly the same protocol. In the case of conventional Pt–Ru bimetallic catalyst, equal volumes of 7.88×10^{-2} M of $RuCl_3{\cdot}xH_2O$ and $H_2PtCl_6{\cdot}6H_2O$ precursor solutions were mixed together and then added to the SiO_2. The nominal metal loadings of all the conventional catalysts were the same as their DMN-derived analogues.

All catalysts studied were activated under flowing H_2 treatment at 300 °C after a slow temperature ramp of 2 °C/min for 2 h followed by cooling to room temperature. This activation protocol was adapted for consistency from a previous study [12] which showed that G4OH dendrimer template could be sufficiently decomposed on an γ-Al_2O_3 support to expose the metal nanoparticles. An O_2–H_2 treatment was purposely avoided due to the severe sintering of Ru particles under O_2 at high temperatures [27–31].

2.3. Transmission electron microscopy and energy dispersive X-ray spectroscopy

High resolution transmission electron microscopy (HRTEM) was conducted using a Philips CM 120 microscope (University of Poitiers, Poitiers, France) operating at 120 kV. Supported Pt–Ru/SiO_2 catalysts were finely crushed and dispersed in methanol (ultrasonically) before subsequent deposition and ambient drying onto a copper grid coated with a carbon. Histograms of particle size distribution were obtained by measuring at least 100 randomly selected particles from at least 6 different micrographs for any sample analyzed. The volume-surface mean diameter was calculated from the following equation:

$$\overline{D} = \sum_i^N N_i D_{p,i}^3 \Big/ \sum_i^N N_i D_{p,i}^2$$

where N_i is the number of particles with a diameter $D_{p,i}$.

Energy dispersive X-ray spectroscopy (EDS) analysis was utilized to measure the elemental composition of individual-supported bimetallic Pt–Ru nanoparticles with a JEOL 2100F 200 kV FEG-STEM/TEM equipped with a CEOS C_s corrector on the illumination system. The geometrical aberrations were measured and controlled to provide less than a $\pi/4$-phase shift of the incoming electron wave over the probe-defining aperture of 15.5 mrad. In EDS analysis, the incident probe beam was focused on a single metallic particle and the X-ray fluorescence generated by this specific particle was detected. Quantitative analyses were based on the characteristic X-ray fluorescence lines of Pt and Ru.

2.4. X-ray diffraction

The crystallographic structures of powder catalysts were obtained by X-ray diffraction (XRD) on a desktop X-ray diffractometer (Rigaku MiniFlex II), using a Cu Kα-monochromatized radiation source (λ = 1.54045 Å) operating at 30 kV and 15 mA. The Bragg angular region (2θ) between 25° and 60° was explored with a slow step size of 0.05°/min due to the extremely low metal loading (~0.5 wt % of Pt and less than 0.2 wt % of Ru for all the three bimetallic catalysts). The peaks were analyzed by JADE 8.5 software.

2.5. O_2–H_2 titration studies

Temperature-programmed O_2–H_2 titration studies were conducted using a gas flow system equipped with a quadruple mass spectrometer as the analytical detector (Leybold Inficon, Model type TSPTT300). All the samples were reduced *in-situ* in flowing H_2 (50 cc/min) at 300 °C for 2 h followed by He (50 cc/min) purging at the same temperature for another 2 h to remove any residual H_2. The catalyst was then cooled to room temperature in flowing He. A temperature-programmed oxidation (TPO) experiment was first conducted in flowing 1% O_2 in He at a ramp rate of 5 °C/min up to 300 °C to dissociatively adsorb O_2 onto exposed metal particle surfaces. The sample was then cooled to room temperature in the same gas flow, followed by Ar purging for 30 min to remove the residual oxygen in the system. H_2 titration measurements were performed at room temperature as follows: pulses of 10% H_2/Ar (0.516 mL STP) were dosed over the catalysts until several successive mass spectral H_2 peaks showed the same peak height. Since water generated by this step will re-adsorb on the support surface at 25 °C, an extra "water removal" stage was used to heat the sample in flowing pure Ar with a ramp of 5 °C/min up to 300 °C. The "*dry*" catalysts were then cooled in flowing Ar to room temperature for temperature-programmed reduction which was executed as follows: 1% H_2/Ar was flowed through the sample at 50 cc/min while the sample was heated to 300 °C at a constant ramp of 5 °C/min. The H_2O^+ signal (m/e = 18) was monitored during this procedure.

In addition to the above temperature-programmed O_2–H_2 titration measurements, the total amount of oxygen adsorbed on the catalysts was confirmed by using a Micromeritics 2920 dynamic chemisorption system. In this measurement, the catalyst was oxidized in 1% O_2/He up to 300 °C at a ramp of 5 °C/min (as above) and cooled to 250 °C in the same gas flow. After purging with pure Ar for 30 min to remove the residual O_2, H_2 doses were pulsed over the catalyst to titrate the oxygen precovered on its surface until several successive H_2 peaks of equal area were observed.

2.6. Temperature-programmed desorption

Temperature-programmed desorption (TPD) of crotonaldehyde was performed using an Altamira AMI-200 system at Oak Ridge National Laboratory as follows. After *in-situ* reduction in flowing H_2 at 300 °C for 2 h as described before, a 5% crotonaldehyde in He gas mixture was passed over the catalyst surface at room temperature. Adsorption of crotonaldehyde was considered complete when the mass intensities for species of m/e = 39, 41, 42, 69, and 70, indicative of crotonaldehyde, were constant. A He gas flow of 100 mL/min was used for 60 min to purge the residual crotonaldehyde from the system. The temperature of the sample was then

ramped at 20 °C/min from room temperature to 500 °C in the same He flow, followed by holding at this temperature for 30 min. Desorption products were analyzed by mass spectrometer for the same five species (m/e = 39, 41, 42, 69, and 70).

2.7. Catalytic evaluation

Selective hydrogenation of 3,4-epoxy-1-butene (EpB) was performed in a 100 mL, gold-coated stainless steel semi-batch autoclave reactor (Autoclave Engineers). A 4-port valve was used to flush the residual liquid remaining in the sample dip tube back into the reactor after sampling to ensure that no liquids were left in the metal tubing between sample collections at different time intervals. Freshly reduced catalyst (typically 300 mg) and 80 mL of hexane (99.5% purity minimum, HPLC grade, VWR) were placed in the reactor. The reactor was flushed three times with pure hydrogen at room temperature before being pressurized to a constant H_2 pressure of 300 psig that was maintained during the reaction period. After reaching the reaction temperature of 80 °C, the reaction was initiated by starting the agitation (rotation speed = 1000 rpm)

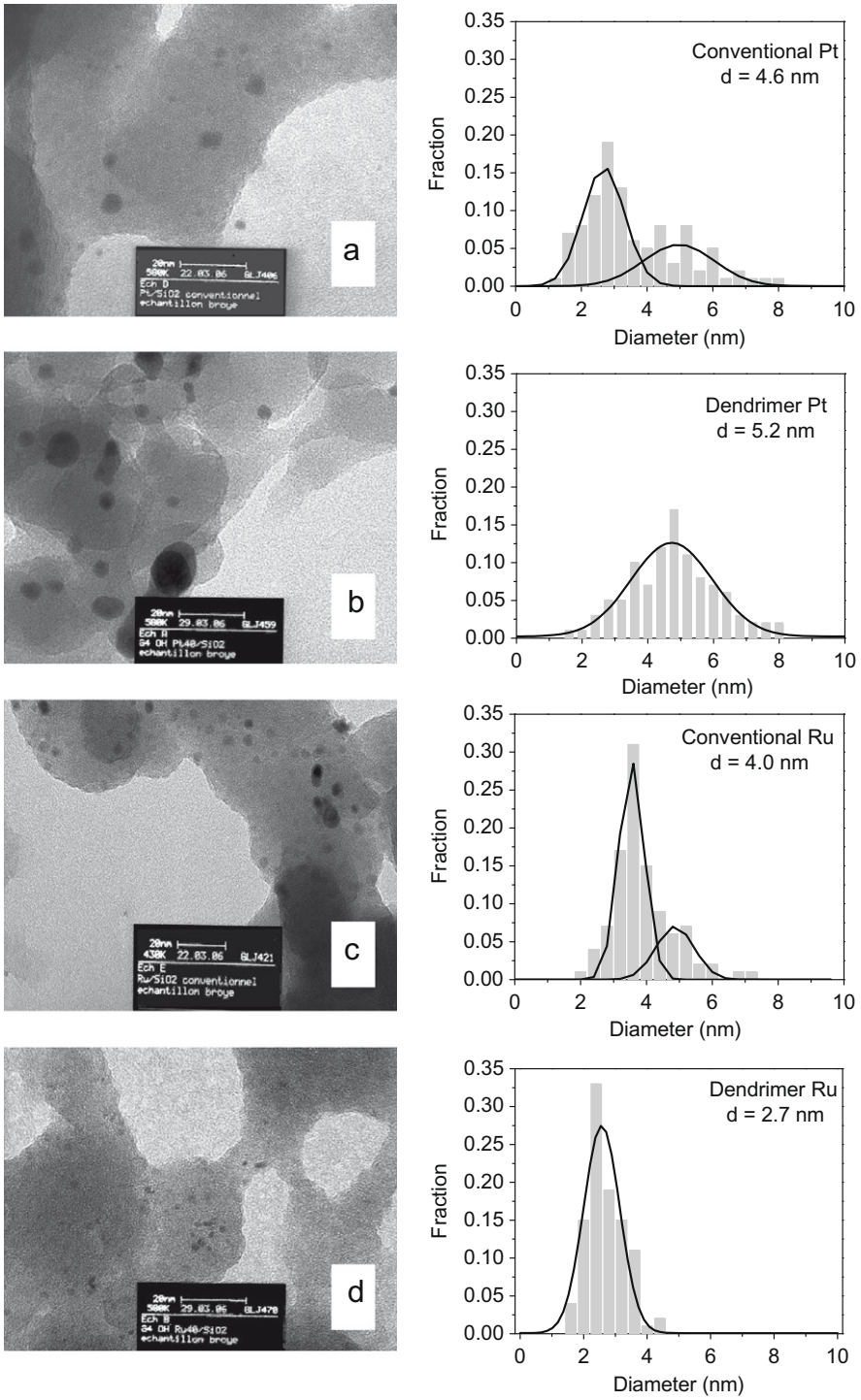

Fig. 3. HRTEM images and histograms of (a) conventional Pt/SiO_2, (b) dendrimer-derived Pt/ SiO_2, (c) conventional Ru/SiO_2, and (d) dendrimer-derived Ru/SiO_2.

and injecting 3,4-epoxy-1-butene (EpB) from a high-pressure liquid pump (Spectra-Physics, Isochrom LC pump). The liquid reaction mixture was sampled at different reaction times and analyzed by gas chromatography (HP 5890) using a 30 m long Hewlett Packer DB-wax capillary column. The reaction was continued until there were no significant changes in the concentrations of the reactor contents. A mole balance was used since all reaction products either were isomers of EpB or had molecular weights that only varied by a maximum of 4 amu (70 g/mol for *n*-butanol vs. 66 g/mol for EpB). Closure of the mole balance was always within 10%.

3. Results and discussion

3.1. Particle size, distribution, and composition

HRTEM micrographs of monometallic Pt samples prepared by conventional incipient wetness method and dendrimer-templating method are shown in Fig. 3a and b, respectively. Analysis of these images yields a volume-surface mean diameter of 4.6 ± 1.5 nm for conventional Pt and 5.2 ± 1.3 nm for dendrimer-derived Pt. Their corresponding particle size distributions are plotted in the histograms next to the HRTEM images. The conventional catalyst has an asymmetric distribution with majority (85%) of the particles between 1 and 4.5 nm and the remaining 15% of particles spread out between 4.5 and 8 nm. In contrast, the dendrimer-derived Pt exhibits a more symmetric distribution, with ca. 50% of particles between 1 and 4.5 nm. Conventional Ru (Fig. 3c) has ~30% larger volume-surface mean diameter (4.0 ± 0.8 nm) and an obviously broader particle size distribution than dendrimer-derived Ru (Fig. 3d), with an average particle size of 2.7 ± 0.6 nm.

There are two explanations for the discrepancy in the role of dendrimer in influencing Pt and Ru particle size and size distribution. One possibility is the much higher mobility of Pt atoms during the elevated temperature H_2 thermal treatment on SiO_2, which causes severe sintering of Pt clusters. Indeed, it has been demonstrated that sintering of metal nanoparticles takes place during the deposition of dendrimer–metal nanocomposites (DMNs) onto supports and in the subsequent elevated temperature H_2 thermal treatment for dendrimer shell removal. In particular, sintering of γ-Al_2O_3-supported Pt nanoclusters during the dendrimer thermal removal step is substantially larger than that observed for Ru particles on the same support [8,15]. Thus, highly mobile Pt atoms/

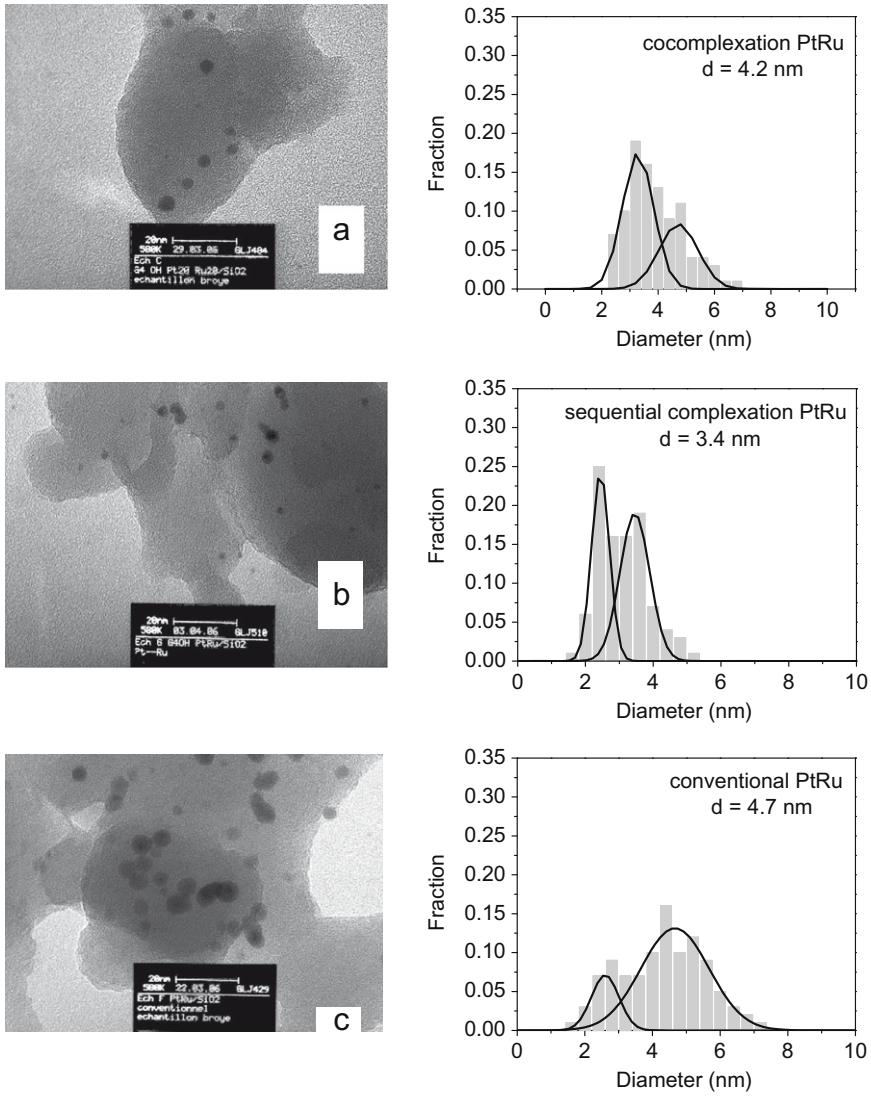

Fig. 4. HRTEM images and histograms of (a) dendrimer-derived $PtRu/SiO_2$ by co-complexation method, (b) dendrimer-derived $PtRu/SiO_2$ by sequential method, and (c) $PtRu/SiO_2$ by conventional incipient wetness method.

clusters may escape from the dendrimer interior and agglomerate together to form larger particles. This in turn results in particle size similar to its conventional counterpart. In contrast, less mobile dendrimer-derived Ru particles are strongly bonded to the support, yielding smaller particle size and narrower distribution. This differing sintering behavior for Pt and Ru has implications for the bimetallic catalyst synthesis. For example, Alerasool and co-workers [32] also reported that bimetallic Pt–Ru/SiO_2 catalysts synthesized by co-impregnation of $H_2PtCl_6{\cdot}6H_2O$ and $RuCl_3{\cdot}3H_2O$ precursors were Pt surface-enriched. They attributed this to the Pt precursor being more mobile on the silica surface than to the Ru precursor in flowing H_2 reduction treatment at 400 °C.

Fig. 4 shows HRTEM images and histograms of the three bimetallic Pt–Ru catalysts synthesized by (a) co-complexation, (b) sequential, and (c) conventional incipient wetness methods. It is apparent that the conventional Pt–Ru catalyst has a larger volume-surface mean diameter and broader size distribution than the two dendrimer-derived Pt–Ru catalysts. This implies that G4OH PAMAM dendrimer exerts a measure of control over particle formation. Energy dispersive X-ray spectroscopy (EDS) was utilized to obtain compositions of individual particles for the three bimetallic Pt–Ru catalysts. At least 10 particles with various sizes were randomly selected from each catalyst. All particles examined in the three catalysts are bimetallic, while monometallic particles consisting of either Pt or Ru were not found. The average percentages of Pt present in the catalysts are similar to 60% average elemental composition obtained via atomic absorption spectroscopy (AAS), albeit with some significant scatter.

3.2. Nanoparticle bulk crystallinity

X-ray diffraction (XRD) patterns of the dendrimer-derived monometallic Pt catalyst and the three bimetallic catalysts are shown in Fig. 5. The conventional Pt catalyst has an identical XRD pattern with its dendrimer-derived partner, and is therefore not shown. Monometallic Ru catalysts, both conventional and dendrimer-derived, did not exhibit any feature due to very low weight loading (~0.5 wt %). It is well known that Pt has a face-centered cubic (f.c.c.) structure. Therefore, the two prominent peaks in dendrimer-derived monometallic Pt at $2\theta = 39.78°$ and 46.08° can be assigned to Pt (1 1 1) and Pt (2 0 0) phases, respectively. Comparing the curves, a slight shift to higher Bragg angles and a broadening of the peak width were observed for the Pt (1 1 1) peak in all three bimetallic Pt–Ru catalysts, especially in the case of the co-complexation sample. This indicates that PtRu alloys have been formed by the substitution of Pt atoms in the lattice with smaller Ru atoms, which causes a decrease in the dimension of the Pt unit cell [33–37].

Pt (1 1 1) and (2 0 0) peak positions extracted from a four parameter least squares fit to a Gaussian function with linear background subtraction are shown at the columns in Table 2. Based on Bragg's law, lattice constants of the Pt unit cell for the three bimetallic PtRu alloys can be calculated using both diffraction peaks and the results are shown in the same table. According to the Vegard's law for a PtRu alloy, the value of the Pt lattice parameter must decrease when Ru content increases, and a linear relation exists (at constant temperature) between the Pt crystal lattice parameter and the Ru concentration in the bimetallic phase [38]. Vegard's law can be applied to unsupported alloys readily. However, it is difficult to evaluate the alloying constants for supported alloys [39]. One reason is that the lattice constant for supported Pt is shorter than that for unsupported Pt due to Pt–support interactions. To estimate the Ru atomic fraction value for supported alloys, an assumption was made that the dependence of the lattice parameter on Ru content for supported alloy is similar to that of the unsupported alloy.

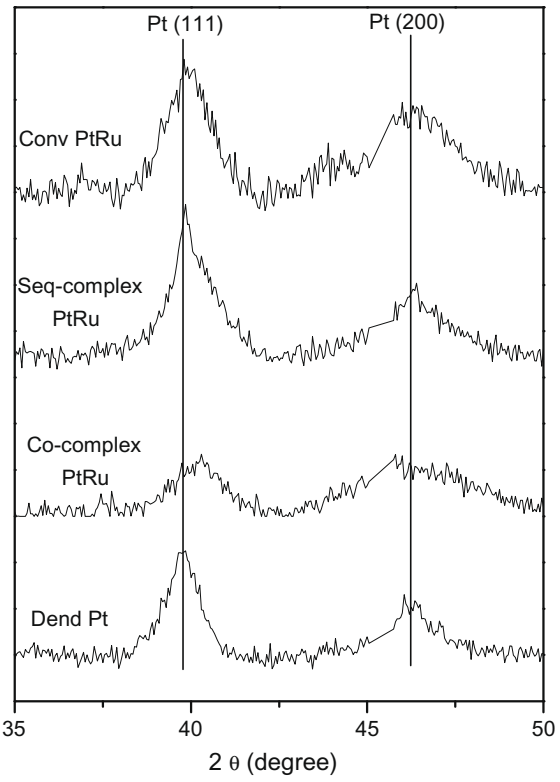

Fig. 5. X-ray diffractograms of silica supported (a) dendrimer-derived monometallic Pt catalyst and Pt–Ru bimetallic catalysts prepared by (b) co-complexation, (c) sequential complexation, and (d) conventional incipient wetness methods.

Based on the assumption above, Vegard's law can be expressed by

$$a_{PtRu} = (1 - x_{Ru}) \cdot a_{Pt} + x_{Ru} \cdot a_{Ru} \quad (1)$$

where a_{PtRu}, a_{Pt} and a_{Ru} are lattice constants for PtRu alloy, pure Pt and pure Ru. x_{Ru} is Ru atomic fraction in the alloy. The equation above can be further simplified as

$$a_{PtRu} = a_{Pt} - x_{Ru} \cdot (a_{Pt} - a_{Ru}) \quad (2)$$

where $(a_{Pt} - a_{Ru}) = 0.124$ Å is a constant obtained from unsupported PtRu alloy [35,39]. Such Ru atomic fraction estimates for the three bimetallic samples are listed at right-most column in Table 2. The co-complexation bimetallic sample has the highest alloying degree with 27% Ru content in its PtRu alloy phase. In contrast, the conventional sample has the lowest alloy degree with only 9% Ru, with the sequential falling in between at 12%.

3.3. Surface site quantification

The type and number of surface sites on bimetallic nanoparticles were probed by hydrogen titration of adsorbed oxygen. The adsorbed oxygen can be titrated from Pt at low temperatures (<100 °C), while significantly higher temperature is required for Ru [40,41]. Therefore, the catalysts were examined by room temperature and temperature-programmed O_2–H_2 titration to determine the temperature profile of the reduction reaction, and thus the distribution of various types of surface sites.

Oxygen precovered on conventional Pt/SiO_2 was titrated by pulse dosing 10% H_2/Ar at room temperature. The titration procedure was considered to be completed when two successive H_2 peaks exhibited identical heights. Fig. 6a shows the mass spectrometer H_2^+ signal ($m/e = 2$) with respect to time. After four injections, there was no more H_2 consumption, indicating that the room

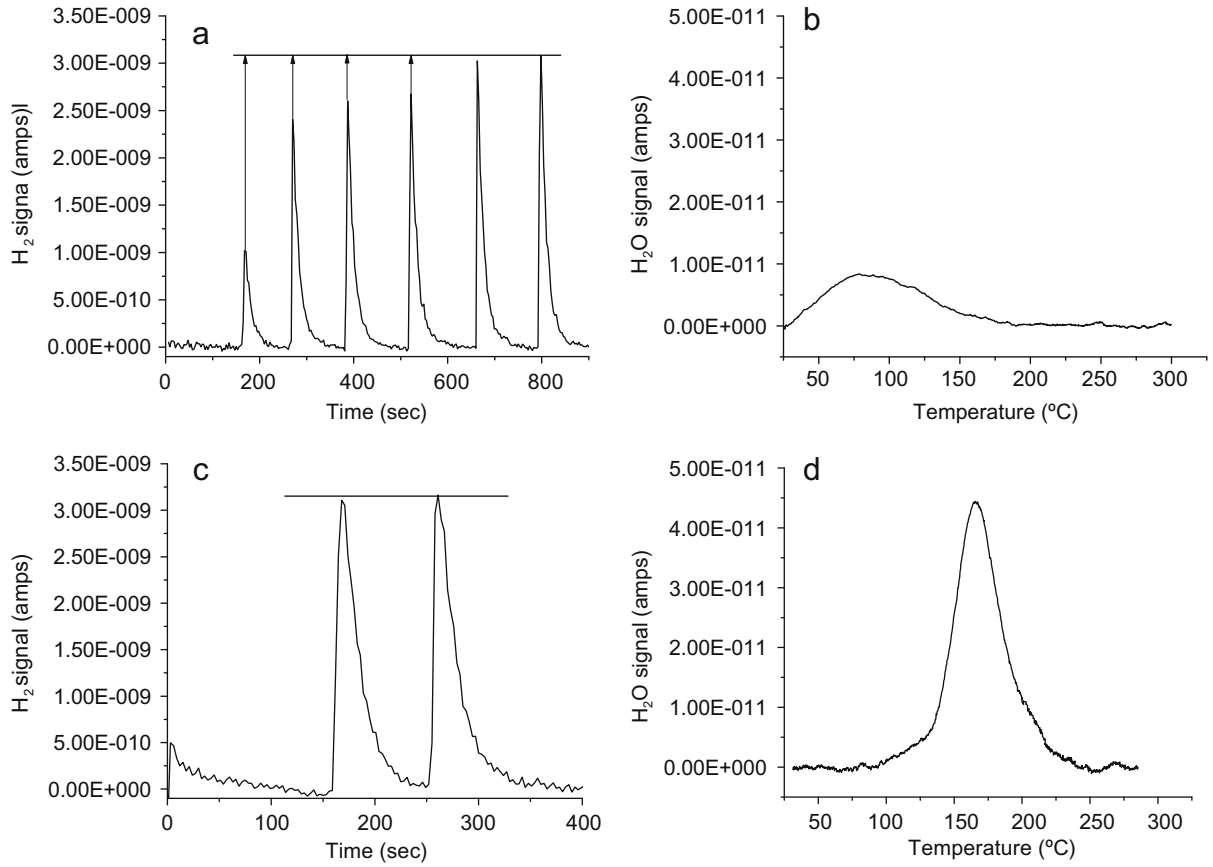

Fig. 6. Temperature-programmed H_2 titration measurement on conventional Pt/SiO_2 at (a) room temperature by pulse dosing of H_2 and (b) as a function of temperature during continuous flowing of H_2; on conventional Ru/SiO_2 at (c) room temperature by pulse dosing H_2, and (d) as a function of temperature during continuous flowing of H_2.

temperature titration was complete. However, only part of the adsorbed oxygen atoms were titrated at room temperature and a higher temperature is needed to remove them entirely. Fig. 6b shows the H_2O^+ (m/e = 18) signal during a ramped heating of conventional Pt/SiO_2 in H_2 from 25 to 300 °C, revealing a broad water desorption peak at 80 °C. However, the total amount of oxygen titrated from this step was much smaller than that titrated at room temperature, as expected. Similar temperature-dependent H_2 titration studies were accomplished on conventional Ru/SiO_2. As shown in Fig. 6c, H_2 consumption is not observed indicating that adsorbed oxygen on Ru is unable to be titrated at room temperature. Temperature-programmed H_2 titration of the same conventional Ru/SiO_2 from 25 to 300 °C in 1% H_2/Ar is shown in Fig. 6d. Water evolution was detected from 100 to 250 °C, with a maximum at 165 °C. Therefore, adsorbed oxygen atoms on Ru sites are completely inactive under 100 °C, indicating more stable adsorption on the oxophilic Ru (and perhaps some presence of more stable Ru oxide species).

Temperature-programmed titration studies on the other catalysts were also performed, and the results for all the catalysts are plotted from 25 to 300 °C in Fig. 7. Oxygen atoms precovered on the two monometallic Pt/SiO_2 catalysts were mostly removed at room temperature by pulse dosing 10% H_2, and therefore relatively flat lines are observed in Fig. 7. In contrast, Ru interacts with oxygen atoms more strongly compared to Pt, resulting in large peaks in the high temperature region. Water peak positions of the three bimetallic catalysts sit in between the two monometallics, which indicates that there are both Pt- and Ru-like sites on the bimetallic surfaces.

Water evolution curves for all the catalysts were fitted with several Gaussian functions to distinguish different types of surface sites, as shown by the dashed lines in Fig. 7. The center temperatures of each type of site as well as their relative amounts are reported in Table S1 (see Supplementary material). For instance, analysis of the water desorption curves for the conventional Pt/SiO_2 catalyst reveals two peaks centered at 70 and 105 °C that likely represent two types of Pt sites. Similarly, three types of Ru surface sites centered at 132, 158, and 187 °C can be classified from the conventional Ru/SiO_2 catalyst. All these surface sites can be categorized into two regions based on their center temperatures: a lower region from 25 to 110 °C and a higher region above 110 °C. The former have been designated as "Pt-like" and the latter as "Ru-like", and the areas under these curves have been used to estimate (see Supplementary material) the number of Pt and Ru surface atoms in each catalyst and the surface compositions (Table 3). For comparison, bulk compositions obtained from atomic absorption spectroscopy (AAS) are also listed in Table 3. It is important to mention that surface compositions obtained as the result of temperature-programmed O_2 and H_2 titration studies described above would represent an average of all particles in the catalyst. Nevertheless, the EDS results suggest that the large majority of the particles are indeed bimetallic in nature.

It is not surprising to observe Pt surface enrichment in bulk PtRu alloys due to the relatively lower enthalpy of vaporization of Pt (510 kJ/mol) compared to Ru (595 kJ/mol) and negligible heat of mixing of the two metals [42]. Gasteiger et al. [43] reported a nearly constant 87% Pt surface composition for bulk Pt content varying from 20% to 60%. In supported PtRu alloy, the surface enrichment also depends on the metal–support interaction in addition to the enthalpy of vaporization of the two metals. Since SiO_2 is considerably acidic, when co-depositing two metal precursor solutions ($RuCl_3$ and H_2PtCl_6) onto the support without dendrimer

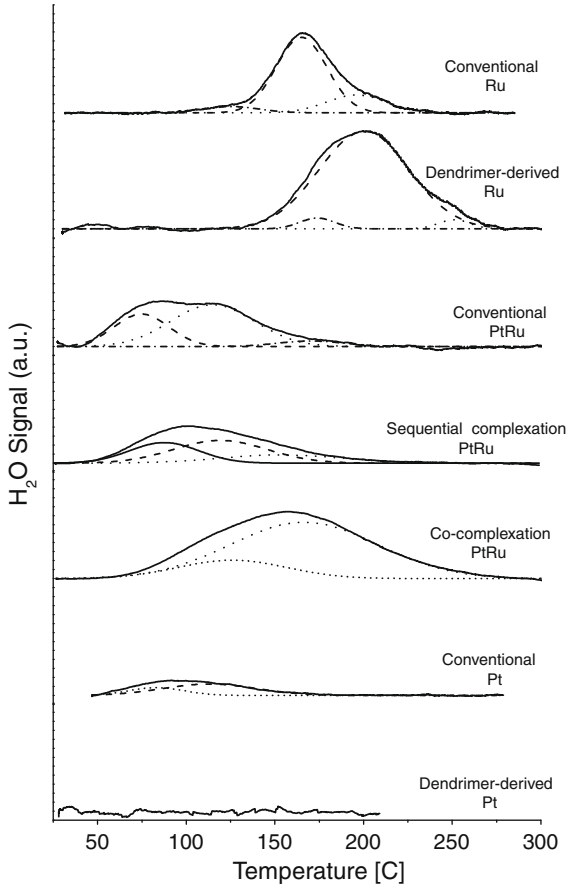

Fig. 7. Temperature-programmed H_2 titration over different catalysts.

template (as for conventional PtRu/SiO_2), it exchanges protons for cations (Ru^{3+}) but not anions ($PtCl_6^{2-}$) to form ligand bonds. Therefore, the Pt precursor is more mobile than the Ru precursor on the SiO_2 surface during H_2 reduction, and the particles that are surface-enriched with Pt are formed. Such a Pt-enriched surface for conventional PtRu bimetallic catalysts is in excellent agreement with that in the reported data for similar catalysts [32,44–46]. In contrast, the surface compositions of the dendrimer-derived sequential complexation catalyst are almost identical to its bulk composition. Finally, dendrimer-derived co-complexation sample has a Ru-enriched surface with the surface composition of about 50–50% Pt–Ru active sites. This is consistent with the presence of PtRu alloy as indicated by the XRD data, wherein the sample with the higher Ru atomic fraction in its PtRu alloy phase has more surface Ru active sites presented on its surface.

It is also interesting to compare the average particle sizes of monometallic Pt and Ru catalysts calculated based on metal dispersions with those calculated from HRTEM data (Table 1). From this comparison, it is clear that the results acquired from the two methods are close for conventional monometallic catalysts. However, in the case of the dendrimer-derived Pt, the particle size estimated from the titration method is much larger than that determined from HRTEM. This discrepancy is attributed to residual dendrimer fragments that cover a part of the metal surface sites, thus leading to a larger calculated average particle size. Given that the optimal treatment to remove PAMAM–OH from Pt–DMNs involves a high temperature oxidation step [9,16], the single H_2 treatment here is likely not enough for full removal. In contrast, the H_2 treatment is optimized for Ru–DMNs, which explains the very good agreement for the Ru samples.

Table 1
Metal particle size measured by HRTEM and $O_2 + H_2$ titration methods.

Catalysts	Volume surface mean diameter[a] from HRTEM (nm)	Average particle size from $O_2 + H_2$ titration (nm)
Conventional Pt	4.6 ± 1.5	4.4
Conventional Ru	4.0 ± 0.8	3.3
Conventional PtRu	4.7 ± 1.2	–
Dendrimer-derived Pt	5.2 ± 1.3	21.0
Dendrimer-derived Ru	2.7 ± 0.6	3.3
Co-complexation PtRu	4.2 ± 1.1	–
Seq. complexation PtRu	3.4 ± 0.8	–

[a] As described in the text.

3.4. Catalytic evaluation

Before evaluating this family of catalysts for hydrogenation of EpB, blank experiments were performed on the silica support to estimate its influence on the reaction. Concentrations of all the products increased very slowly, while the concentration of EpB decreased slowly, indicating only marginal activity for the silica support. This low activity is most likely due to the weak acid sites of the silica that catalyze EpB isomerization reactions. However, over the time scales used to evaluate the supported catalysts, the contribution of SiO_2 to the product formation rates was found to be negligible. The mole balance of the reaction is essentially constant during the entire reaction period, indicating that all formed products were detected. In order to minimize internal mass transfer limitations, all the catalysts were ground to fine powder before use. Five stirring speeds of 100, 300, 700, 1000, and 1830 rpm were examined for external mass transfer limitation study on a test Pt/SiO_2 catalyst. The reaction rates were essentially independent of stirring rates over the entire range of stirring speeds. As a result, 1000 rpm was selected as the stirring rate for all catalytic runs. Finally, it has also been shown that EpB adsorbs strongly on most metals through multiple chemical bonds with the surface [19,23,47]. This strong adsorption has resulted in deactivation during gas-phase reactions where EpB is either a reactant or a product [24,26,48]. However, batch experiments involving multiple injections of EpB over the same catalyst showed no significant deterioration in catalytic activity (see Fig. S1 in Supplementary material), suggesting that this is likely not a problem in the present study.

Batch kinetic data were obtained for all catalysts during hydrogenation of EpB. As an example, Fig. 8 shows the concentration profile of the reactant and all the products plotted as a function of time for (a) conventional Pt/SiO_2 and (b) PtRu/SiO_2 by co-complexation method. In both plots, the concentration of EpB decreased rapidly, and was completely consumed after a certain period of time. The concentrations of crotyl alcohol, 3-buten-1-ol, and crotonaldehyde passed through maxima indicating that they were reaction intermediates. The reaction end products are butylene oxide (BO), *n*-butanol, and *n*-butyraldehyde, whose concentrations monotonically increase and then stabilize with increasing reaction time. The initial reaction rates of EpB were determined from such concentration-time data by taking the slope of the first two data points at $t = 0$ and 5 min. Calculation of EpB turn over frequencies (TOFs) was based on the total metal active surface sites (Pt-like + Ru-like) as listed in Table 3. Dividing the initial reaction rate of each product by the initial reaction rate of EpB yielded initial instantaneous selectivities. Such selectivities were calculated individually for all the six products, butylene oxide (BO), crotonaldehyde, 3-buten-1-ol, *n*-butanol, *n*-butyraldehyde, and crotyl alcohol.

3.5. Catalytic activity

Table 4 lists the TOFs measured for the entire family of catalysts. Both conventional and dendrimer-derived monometallic Ru

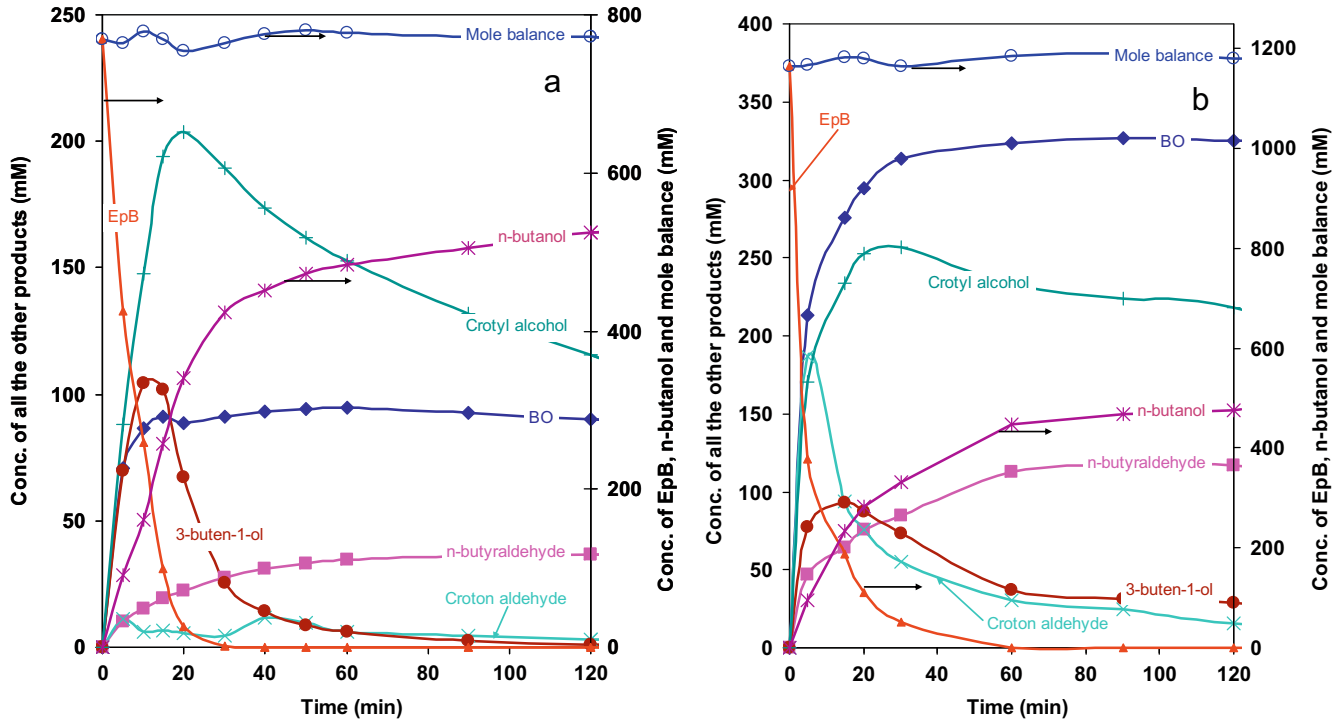

Fig. 8. Concentration profile obtained during the EpB hydrogenation reaction on (a) conventional Pt/SiO_2 and (b) dendrimer-derived co-complexation $PtRu/SiO_2$ catalyst.

Table 2
Pt lattice constants and estimated Ru atomic fractions in PtRu alloys.

Catalysts	Pt (1 1 1) peak position (°)	Pt (2 0 0) peak position (°)	Lattice constant (Å)	Ru atomic fraction in PtRu alloy
Dendrimer-derived Pt	39.78	46.08	3.929 ± 0.010	–
Conventional PtRu	39.93	46.31	3.912 ± 0.007	0.09
Co-complexation PtRu	40.20	46.56	3.890 ± 0.011	0.27
Seq. complexation PtRu	39.98	46.36	3.908 ± 0.008	0.12

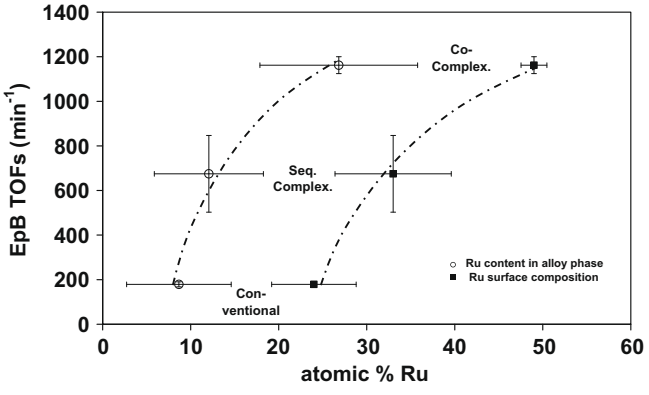

Fig. 9. EpB TOFs as a function of atomic Ru percentage in the PtRu alloys (circles) and on the surface (squares) of co-complexation, sequential complexation, and conventional PtRu bimetallic catalysts. The dashed lines are provided to illustrate the trends.

catalysts are much less active than their Pt counterparts. This is most likely linked to the relative inability of Ru to dissociatively adsorb H_2 at reaction temperatures of 80 °C. Consequently, higher temperatures (>373 K) are typically used for reactions or processes involving H_2 dissociation. This is particularly the case for small particle sizes (<4 nm) such as those prepared in this study [28,41,49,50]. In contrast, H_2 dissociatively adsorbs on Pt surfaces readily at room temperature, supplying enough adsorbed H atoms for rapid hydrogenation to occur.

The EpB TOF on the dendrimer-derived Pt catalyst is about twice that for conventional Pt, which has a majority (85%) of its particles between 1 and 4.5 nm and the remaining 15% spread out between 4.5 and 8 nm. In contrast, the dendrimer-derived Pt has only 50% of its particles between 1 and 4.5 nm and the other half larger than 4.5 nm (as shown in Fig. 3). A likely explanation for this behavior is that EpB hydrogenation is a structure sensitive reaction that requires a large number of highly coordinated crystalline sites (e.g., exposed Pt (1 1 1) planes) to facilitate the adsorption of both EpB and H atoms in close proximity to each other. Since the dendrimer-derived Pt catalyst has a higher percentage of large size particles compared to its conventional counterpart, more of these crustal planes are exposed, thus resulting in higher TOFs for EpB conversion.

Clearly, the dendrimer-derived PtRu bimetallic catalyst prepared by the co-complexation method is the most active of the three bimetallic catalysts examined. The catalyst prepared by sequential complexation is a factor of two less active, and conventionally prepared one is yet another factor of two less active. The higher activity for the co-complexation catalyst can result from (a) more exposed Pt monometallic sites that therefore yield higher activity per combined surface metal site (i.e., Pt + Ru), (b) bimetallic PtRu alloy sites have been created that have higher intrinsic activity, or (c) a combination of the two hypothesis. It is easy to rule out the first hypothesis by checking the exposed metal sites

Table 3
Metal surface sites, surface composition, actual metal loading, and bulk composition.

Catalysts	Site amount (atoms/g cat) $\times 10^{-18}$			Surface composition		Metal weight loading[a]		Bulk composition[a]	
	Pt-like sites	Ru-like sites	Total sites	Pt (%)	Ru (%)	Pt (%)	Ru (%)	Pt (%)	Ru (%)
Conventional Pt	7.5	–	7.5	100	–	0.95	–	100	–
Conventional Ru	–	12	12	–	100	–	0.5	–	100
Conventional PtRu	6.6	2.2	8.8	76	24	0.53	0.16	63	37
Dendrimer-derived Pt	2.1	–	2.1	100	–	1.19	–	100	–
Dendrimer-derived Ru	–	9.9	9.9	–	100	–	0.42	–	100
Co-complexation PtRu	3.4	3.2	6.6	51	49	0.56	0.19	60	40
Seq. complexation PtRu	3.9	1.9	5.9	67	33	0.57	0.18	62	38

[a] Obtained by elemental analysis.

Table 4
EpB TOFs for all catalysts.

Catalyst	EpB TOFs (min^{-1})
Conventional Pt	762 ± 49
Dendrimer-derived Pt	1486 ± 70
Conventional Ru	21 ± 0
Dendrimer-derived Ru	29 ± 0
Conventional PtRu	179 ± 11
Co-complexation PtRu	1162 ± 38
Sequential complexation PtRu	675 ± 172

reported in Table 3. The co-complexation sample has neither the highest number of Pt sites, nor the total metal exposed sites on its surface. However, the second hypothesis appears to be supported by the XRD analysis (cf. Table 2). As shown in Fig. 9 (circles), the initial EpB TOFs of the bimetallic catalysts exhibit a strong dependence on the atomic Ru composition in their PtRu alloy phases. The most active co-complexation sample has the highest alloying degree with 33% Ru, while the lowest activity conventional PtRu alloy contains only 12% Ru.

This "bimetallic site" supposition is further strengthened by consideration of the relative distribution of Pt-like and Ru-like surface sites in each catalyst (cf. Table 3). A plot of EpB TOFs vs. the Ru surface composition is also shown in Fig. 9 (squares). It is clear that there is also a strong relationship between reactivity and the atomic surface composition. This trend suggests the existence of bimetallic surface PtRu bimetallic sites that activate EpB conversion. Electronic effects between Pt and Ru are known to be small due to their similar electronegativities [51]. Since Ru sites are essentially inactive relative to Pt, Ru dilution of Pt ensembles would be expected to depress the activity. However, more Ru atoms are exposed on the surface in co-complexation case, which has the highest EpB TOF. The enhanced activity of EpB conversion is therefore more likely the result of a bifunctional effect. Ru is oxophilic [15,51], which will facilitate the adsorption of the epoxy group of EpB molecule. The neighboring Pt site then could more readily interact with the C=C bond of adsorbed EpB and other intermediates. Thus, the existence of such bimetallic sites, as is especially the case with the co-complexation catalyst, increases the reactivity of EpB.

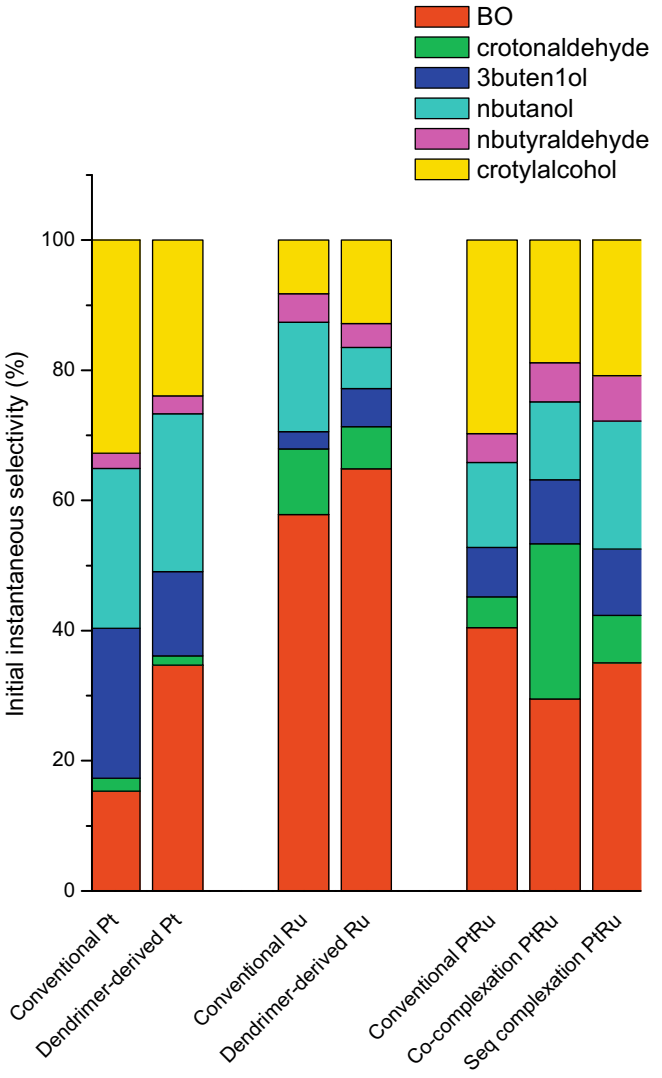

Fig. 10. Initial instantaneous selectivities to all products during EpB hydrogenation over various catalysts.

3.6. Selectivity

The initial instantaneous selectivities to all the six products, which are butylene oxide (BO) (red)[1], crotonaldehyde (green), 3-buten-1-ol (blue), *n*-butanol (cyan), *n*-butyraldehyde (magenta), and crotyl alcohol (yellow) for all catalysts are shown in the bar plots of Fig. 10. For the monometallic Pt catalysts, which are active C=C hydrogenation catalysts [52], significant selectivity to products other than BO was observed. Furthermore, BO was formed by a parallel pathway and is a stable end product, suggesting that a C=C bond is required for adsorption of EpB-derived intermediates on Pt surfaces. The result is consistent with the results of Bartok et al. [19] and Schaal et al. [24] , who have reported that EpB can adsorb on Pt at both the C=C bond and the epoxide oxygen. Bartok reported that BO was the main product at gas-phase reaction conditions of 301 K, with P_{H_2} = 20 kPa. Initial instantaneous selectivity to crotonal-

[1] For interpretation of color in Fig. 10, the reader is referred to the web version of this article.

dehyde was extremely low (2–3%), indicating either that crotonaldehyde was extremely reactive or that hydrogenation to the other products proceeded through the 3-buten-1-ol route.

In general, the selectivities for the bimetallic catalysts are somewhat similar, although the $PtRu/SiO_2$ catalyst produced by co-complexation has a much higher initial selectivity to crotonaldehyde. This suggests that isomerization of adsorbed EpB to form crotonaldehyde is favored, and that subsequent hydrogenation to other products preferentially occurs through crotonaldehyde, as opposed to 3-butene-1-ol. This particular catalyst does have a strong affinity for crotonaldehyde adsorption, as shown by the results of crotonaldehyde TPD studies (see Supplementary material, Fig. S2 and Table S2). In these studies, the co-complexation catalyst had by far the highest uptake of crotonaldehyde as well as the strongest interaction based on the temperatures of the desorption peaks. Thus, the bimetallic sites produced by the co-complexation method enhance the adsorption of crotonaldehyde, and thus facilitate the reaction of EpB by this isomerization route.

4. Conclusions

In conclusion, a series of silica-supported monometallic (Pt, Ru) and bimetallic (PtRu) catalysts have been synthesized using both dendrimer–metal nanocomposites (DMNs) and metal salt precursors. They have been characterized by HRTEM, EDS, XRD, and O_2–H_2 titration measurements. Histograms obtained from electron microscopy reveal that the dendrimer-mediated synthesis yields smaller particle sizes and narrower particle size distributions compared with the conventional incipient wetness impregnation for the monometallic Ru and Pt–Ru. In contrast, the Pt shows a larger particle size distribution, consistent with the previous findings. EDS measurements indicate that most (if not all) of the particles are bimetallic in the bimetallic catalysts. While XRD patterns suggest that PtRu alloy phase has been formed in all the three bimetallic catalysts, analysis suggests that the co-complexation sample has the highest Ru content (33%) in its alloy phase. In contrast, conventional PtRu has the least Ru content (12%) in its alloy phase. In concert with these findings, O_2–H_2 titration shows that the co-complexation catalyst has a relatively Ru-enriched surface, while conventional PtRu has a Pt-enriched surface.

Batch kinetics studies of liquid-phase hydrogenation of 3,4-epoxy-1-butene revealed notable differences in the catalytic performance across this family of catalysts. The two dendrimer-derived PtRu bimetallic samples (especially the co-complexation sample) are intrinsically more active than their conventional counterpart. This difference is attributed to a bifunctional performance of the PtRu alloy sites created, and the TOF values are found to correlate strongly with both the alloy composition and the metal surface site distribution. The crotonaldehyde reaction pathway is favored on the co-complexation catalyst, in contrast to the other catalysts that favor the 3-buten-1-ol route. Crotonaldehyde TPD results suggest that this difference is attributed to the relative affinity of these catalysts toward this intermediate. Taken together, these results indicate that the DMN methodology provides a significant measure of control over bimetallic catalyst properties for the PtRu bimetallic system.

Acknowledgments

This work was supported by a grant from the National Science Foundation NIRT award (NSF-0103135). The authors would like to thank Dr. Attilio Siani for assistance with the catalyst synthesis, Dr. Snigdhamayee Praharaj for performing the XRD measurements, and Dr. Gwendoline Lafaye for arranging the HRTEM imaging at the University of Poitiers. Temperature-programmed desorption of crotonaldehyde was performed at Oak Ridge National Laboratory's Center for Nanophase Materials Sciences with assistance from Dr. Zili Wu, and was sponsored by the Scientific User Facilities Division, Office of Basic Energy Sciences, US Department of Energy and finally, two undergraduate students Michelle Casper and Paul Wilkinson for assistance with the catalytic hydrogenation experiments.

Appendix A. Supplementary material

Supplementary data associated with this article can be found, in the online version, at doi:10.1016/j.jcat.2009.11.021.

References

[1] J.H. Sinfelt, Acc. Chem. Res. 10 (1977) 15.
[2] J.H. Sinflet, Bimetallic Catalysts: Discoveries, Concepts, and Applications, John Wiley & Sons, Inc., 1983.
[3] C.T. Campbell, Ann. Rev. Phys. Chem. 41 (1990) 775.
[4] D.A. Tomalia, A.M. Naylor, W.A.I. Goddard, Angew. Chem., Int. Ed. 29 (1990) 138.
[5] J.M. Frechet, Science 263 (1994) 1710.
[6] R.M. Crooks, B.I. Lemon III, L. Sun, L.K. Yeung, M. Zhao, Top. Curr. Chem. 212 (2001) 81.
[7] R.M. Crooks, M. Zhao, L. Sun, V. Chechik, L.K. Yeung, Acc. Chem. Res. 34 (2001) 181.
[8] O.S. Alexeev, A. Siani, G. Lafaye, C.T. Williams, H.J. Ploehn, M.D. Amiridis, J. Phys. Chem. B 110 (2006) 24903.
[9] D.S. Deutsch, A. Siani, P.T. Fanson, H. Hirata, S. Matsumoto, C.T. Williams, M.D. Amiridis, J. Phys. Chem. C 111 (2007) 4246.
[10] D.S. Deutsch, C.T. Williams, M.D. Amiridis, in: J. Regalbuto, (Ed.), Catalyst Preparation, CRC Press LLC, Boca Raton, Fal, 2007, p. 209.
[11] G. Lafaye, A. Siani, P. Marecot, M.D. Amiridis, C.T. Williams, J. Phys. Chem. B 110 (2006) 7725.
[12] G. Lafaye, C.T. Williams, M.D. Amiridis, Catal. Lett. 96 (2004) 43.
[13] H. Xie, J.Y. Howe, V. Schwartz, J.R. Monnier, C.T. Williams, H.J. Ploehn, J. Catal. 259 (2008) 111.
[14] D. Liu, J. Gao, C.J. Murphy, C.T. Williams, J. Phys. Chem. B 108 (2004) 12911.
[15] G. Lafaye, C.T. Williams, O.S. Alexeev, M.D. Amiridis, Manuscript in draft.
[16] D.S. Deutsch, G. Lafaye, D. Liu, B. Chandler, C.T. Williams, M.D. Amiridis, Catal. Lett. 97 (2004) 139.
[17] H. Lang, S. Maldonado, K.J. Stevenson, B.D. Chandler, J. Am. Chem. Soc. 126 (2004) 12949.
[18] N.N. Hoover, B.J. Auten, B.D. Chandler, J. Phys. Chem. B 110 (2006) 8606.
[19] M. Bartok, A. Fasi, F. Notheisz, J. Catal. 175 (1998) 40.
[20] M. Bartók, A. Fási, F. Notheisz, J. Mol. Catal. A: Chem. 135 (1998) 307.
[21] I.S. Cho, B. Lee, H. Alper, Tetrahedron Lett. 36 (1995) 6009.
[22] H. Fujitsu, E. Matsumura, S. Shirahama, K. Takeshita, I. Mochida, J. Chem. Soc. Perkin 1 (1982) 855.
[23] A.S. Loh, S.W. Davis, J.W. Medlin, J. Am. Chem. Soc. 130 (2008) 5507.
[24] M.T. Schaal, A.C. Pickerell, C.T. Williams, J.R. Monnier, J. Catal. 254 (2008) 131.
[25] J.R. Monnier, B.D. Roberts, D.M. Hitch, US Patent 6,180 559, Eastman Chemical Company, USA, 2001.
[26] M.T. Schaal, A.Y. Metcalf, J.H. Montoya, J.P. Wilkinson, C.C. Stork, C.T. Williams, J.R. Monnier, Catal. Today 123 (2007) 142.
[27] G.C. Bond, J.C. Slaa, J. Mol. Catal. 89 (1994) 221.
[28] G.C. Bond, J.C. Slaa, J. Mol. Catal. A: Chem. 96 (1995) 163.
[29] C. Elmasides, D.I. Kondarides, W. Grunert, X.E. Verykios, J. Phys. Chem. B 103 (1999) 5227.
[30] V. Mazzieri, F. coloma-Pascual, A. Arcoya, P.C. L'Argentiere, N.C. Figoli, Appl. Surf. Sci. 210 (2003) 222.
[31] J. Wellenbuscher, M. Muhler, W. Mahdi, U. Sauerlandt, J. Schutze, G. Ertl, R. Schlogl, Catal. Lett. 25 (1994) 61.
[32] S. Alerasool, R.D. Gonzalez, J. Catal. 124 (1990) 204.
[33] A.S. Arico, P.L. Antonucci, E. Modica, V. Baglio, H. Kim, V. Antonucci, Electrochim. Acta 47 (2002) 3723.
[34] C.T. Hsieh, Y.W. Chou, W.Y. Chen, J. Alloys Compd. 466 (2008) 233.
[35] J. Prabhuram, T.S. Zhao, Z.X. Liang, R. Chen, Electrochim. Acta 52 (2007) 2649.
[36] V. Radmilovic, H.A. Gasteiger, P.N. Ross Jr., J. Catal. 154 (1995) 98.
[37] M.-S. Loffler, H. Natter, R. Hempelmann, K. Wippermann, Electrochim. Acta 48 (2003) 3047.
[38] W. Vogel, P. Britz, H. Bonnemann, J. Rothe, J. Hormes, J. Phys. Chem. B 101 (1997) 11029.
[39] E. Antolini, F. Cardellini, J. Alloys Compd. 315 (2001) 118.
[40] G. Blanchard, H. Charcosset, Stud. Surf. Sci. Catal. 4 (1980) 515.
[41] H. Kubicka, React. Kinet. Catal. Lett. 5 (1976) 223.
[42] A.R. Miedema, Philips Tech. Rev. 36 (1976) 217.
[43] H.A.R. Gasteiger, P.N. Ross, E.J. Cairns, Surf. Sci. 293 (1993) 67.
[44] H. Miura, R.D. Gonzalez, J. Catal. 74 (1982) 216.
[45] H. Miura, T. Suzuki, Y. Ushikubo, K. Sugiyama, T. Matsuda, R.D. Gonzalez, J. Catal. 85 (1984) 331.

[46] H. Miura, H. Taguchi, K. Sugiyama, T. Matsuda, R.D. Gonzalez, J. Catal. 124 (1990) 194.
[47] J.W. Medlin, M.A. Barteau, J.M. Vohs, J. Mol. Catal. A: Chem. 163 (2000) 129.
[48] J. Monnier, Stud. Surf. Sci. Catal. 110 (1997) 135.
[49] K. Lu, B.J. Tatarchuk, J. Catal. 106 (1987) 166.
[50] D.O. Uner, M. Pruski, T.S. King, J. Catal. 156 (1995) 60.
[51] A.K. Shukla, A.S. Arico, K.M. El-Khatib, Appl. Surf. Sci. 137 (1999) 20.
[52] S. Nishimura, Handbook of Heterogeneous Catalytic Hydrogenation for Organic Synthesis, John Wiley & Sons, Inc., 2001.